Scale Transformation of Magnetic "Bubble" Arrays: Coupling of Topological Disorder and Polydispersity

M. Seul* and C. A. Murray

The evolution of disorder in response to period adaptation in a hexagonal magnetic bubble array is shown to arise from the proliferation of dislocations and to proceed by means of intermediate states of steadily decreasing hexatic order to an amorphous final state. Remarkably, each dislocation core imposes a size adjustment on bubbles decorating its constituent pair of five- and sevenfold coordinated sites. Topological disorder thus induces intrinsic polydispersity and converts the initially unimodal size distribution into a trimodal one. This intimate interplay between geometry and topology provides an explicit mechanism by which structural disorder arises as a result of frustration.

Domain formation is encountered in a wide variety of condensed matter systems, including thin films of type I superconductors (*1*), ferrofluids (*2*), and ferrimagnetic garnets (*3, 4*), as well as monomolecular amphiphilic (Langmuir) films (*5, 6*) and certain semiconductor and metal surfaces (*7*). Mean-field theories describing domain patterns as a manifestation of a modulated order parameter field yield stripes and cylindrical "bubbles" as the simplest possible realizations of these modulated phases (*4, 6, 7*). These are respectively characterized by a single and a set of three modulation wavevectors, $\mathbf{q}$, whose magnitude depends on the applied field, H, and temperature, T, so that $q \equiv |\mathbf{q}(H,T)|$ or, for constant H, $q \equiv |\mathbf{q}_H(T)|$. The modulation period, $d \equiv 2\pi/q$, is set by the competition of a short-ranged attractive and a long-ranged repulsive interaction of magnetostatic (*1–4*), electrostatic (*6, 7*), or strain-elastic (*7*) origin. However, in most experimental situations, stripe and bubble domain phases are found to adopt disordered configurations rather than simple, ordered ones.

The focus of this report is the nature of the disorder and the disordering process of a hexagonal bubble array subjected to a scale transformation. Tuning of the modulation period of such an array by means of its temperature dependence (*8, 9*) in the presence of a small, constant magnetic field generates strain to which the system must respond by suitably adjusting bubble area and (number) density while maintaining constant net magnetization ("coverage"). Detailed pattern analysis reveals that the transformation of the ordered initial state into an amorphous final state involves a remarkable coupling between "lattice" and "single particle" degrees of freedom. The former are those affected by topological defects, which mediate disordering and melting in systems of rigid particles (*10, 11*). The latter are characteristic of modulated phases whose constituent domains are known to exhibit a variety of domain shape instabilities (*2, 3, 12–15*). The disordering process is mediated by the proliferation of (unbound) dislocations: These generate intermediate bubble array configurations of steadily decreasing hexatic order, with bond-orientational correlations substantially exceeding positional correlations (*16*). An inherent polydispersity concomitantly arises: Local strain relaxation in response to the creation of a dislocation leads to the size adjustment of the five- and sevenfold coordinated bubbles marking ± 1 disclinations (*17*) in the defect core, and dislocation cores are thus decorated by pairs of bubbles of mismatched area. The incipient unbinding of disclination pairs in the final stage of disordering signals the appearance of amorphous order, with comparable positional and orientational correlations of about two nearest-neighbor distances. Lattice expansion thus induces a transformation to an amorphous state, characterized by a trimodal distribution of domain areas (*18*). This is to be contrasted with recent investigations of melting in dilute arrays of monodisperse bubbles, in response to an increase in the applied magnetic field to just below the bubble collapse field (*11*), as well as monodisperse colloids (*10*), in which simple dislocation pair unbinding was followed by disclination pair unbinding.

Domain patterns in magnetic garnet films of composition $(YGdTm)_3(FeGa)_6O_{12}$, grown to a thickness of about 13 μm on single-crystal substrates of gadolinium gallium garnet of (111) orientation, were recorded by polarization microscopy (*8, 11*). The ordered initial bubble array was generated by cooling of the film from the paramagnetic state (*8*) in a small, normal magnetic field ($H \approx 1$ Oe). Subsequent disordering was induced by allowing the system to cool in the applied field, over a period of about 2 hours, from $T \approx 175$°C ($\approx 0.96T_c$, where T_c is the critical temperature) to room temperature. This trajectory closely preserves (to within about ±2%) a constant area fraction ("coverage") of bubbles of about 45%, replicating the condition that applies to experiments on Langmuir films of mixed surfactants (*14, 19*). Patterns were binarized (*20*) and processed to locate domain centroids and evaluate domain area histograms. Construction of the Voronoi diagram of the resulting point pattern facilitated the identification of topological defects (*21*).

Bubble patterns in the course of the disordering process are displayed in Fig. 1. The corresponding Fourier spectra document the (radial as well as azimuthal) broadening of the diffraction spots as topological defects proliferate. These defects are identified as dislocations in the superposition of a fully disordered bubble domain pattern and its Voronoi diagram (Fig. 2A). This construction reveals the

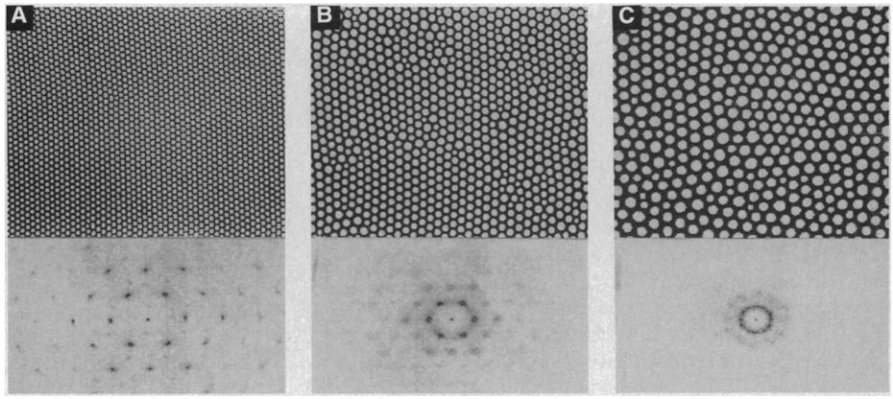

Fig. 1. Magnetic bubble patterns (top) and their respective Fourier spectra (bottom) documenting the evolution of disorder by means of the proliferation of dislocations in response to temperature-mediated period adjustment in a constant magnetic field ($H \approx 1$ Oe) applied normal to the layer plane. The respective modulation periods are (**A**) 9.5 μm, (**B**) 15 μm, and (**C**) 23 μm. The horizontal dimension of each field of view in the top panels is 570 μm.

AT&T Bell Laboratories, Murray Hill, NJ 07974.

*To whom correspondence should be addressed.

strong pairing of five- and sevenfold sites into dislocations, which themselves tend to form pairs and clusters (9). Both the nucleation and the subsequent motion of dislocations rely on transient shape distortions, explicitly involving the elimination of fivefold coordinated bubbles (9). The overlay in Fig. 2A also demonstrates that five- and sevenfold sites coincide with the position of bubbles that are, respectively, smaller than and larger than the bubbles that decorate all sixfold sites, and adopt the (temperature-dependent) optimal area A_6. Polydispersity and topological disorder are thus found to be intimately related.

A record of the number of bubbles, $N \equiv N_H(T)$, in the evolving pattern of linear dimension L_0 reveals that, over most of the experimentally accessible range of temperatures, $N(T)$ exceeds the "optimal" number of domains, $N_6^{opt}(T) \sim L_0^2/A_6(T)$. This indicates that, starting in the ordered state, a decrease in temperature and the ensuing increase (8, 9) in the modulation period, d, initially lead to strain accumulation until, at the yield threshold, the nucleation of defects facilitates the requisite reduction in N. The approximately linear relation between $N(T)$ and $N_6^{opt}(T)$ suggests that the pattern remains at the yield threshold, forming dislocations and eliminating (rows of) particles at a rate sufficient to track the increase in modulation period. The observed (9) scaling of the mean domain area, of the form $\langle A \rangle \sim q^{-2}$, is consistent with the condition of constant coverage.

The unimodal area distribution characterizing the ordered initial state transforms into a trimodal distribution as topological defects continue to proliferate (Fig. 3). The mean area corresponds to sixfold coordinated sites (9), whereas the emergence of the satellites reflects the formation of dislocations containing small fivefold bubbles and large sevenfold bubbles. The distribution displays a marked asymmetry: The ratio of mean areas $\langle A_6 \rangle / \langle A_7 \rangle$ exceeds the ratio $\langle A_5 \rangle / \langle A_6 \rangle$, and the corresponding standard deviations exhibit a systematic increase, $\sigma_5 \leq \sigma_6 \leq \sigma_7$.

The smooth evolution of disorder manifests itself in the steady decrease of the hexatic order parameter $|\psi_6|$ (*11*, *22*) and the concentration, $c_6 \equiv 1 - (N_5 + N_7)/N$, of sixfold coordinated bubbles (Fig. 4A). It is the concomitant increase in the concentration of defects, $1 - c_6$, that leads to the formation of satellites in the area histograms of Fig. 3.

The existence of free dislocations in disordered bubble patterns is consistent with a rapid decay of positional correlations. The observation that disclinations remain tightly bound would suggest hexatic ordering to persist. This expectation is borne out by explicit evaluation of translational and bond-orientational correlation functions (Fig. 4B). This analysis indicates that, throughout most of the regime of pattern evolution probed here, the range (*17*, *23*) of orientational correlations, ξ_6, exceeds that of translational correlations, ξ, as expected for a hexatic state (*10*, *11*, *22*). Notable is the short range of positional

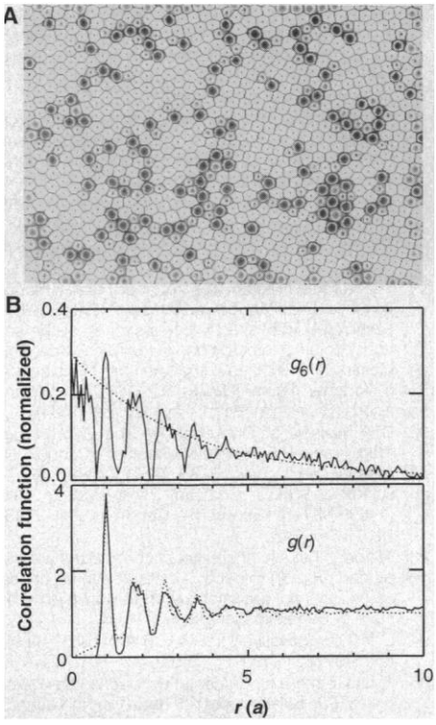

Fig. 2. (**A**) Voronoi diagram constructed from bubble domain centroids of pattern in Fig. 1C. Light and dark gray polygons in the diagram, respectively, indicate five- and sevenfold sites, occupied by bubbles of smaller than optimal and larger than optimal area. The contours of these domains, derived by edge detection from the original pattern, are superimposed. Note the incipient unbinding of disclinations. The horizontal dimension of the field of view is 900 μm. (**B**) Normalized (*10*), azimuthally averaged orientational and translational correlation functions, $g_6(r)$ and $g(r)$, computed from the bubble centers in (A). Dotted lines indicate fits of the envelope of $g_6(r)$ to an exponential, and of $g(r)$ to an azimuthally averaged structure function of a perfect hexagonal lattice with multiplicative exponential decay; the unit of r is the nearest-neighbor distance, a.

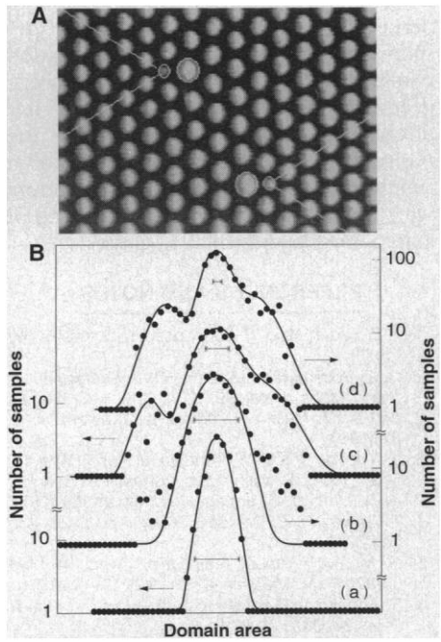

Fig. 3. (**A**) Enlarged section of a nearly ordered bubble domain pattern exhibiting a pair of dislocations whose core is composed of a pair of bubbles of nonoptimal size. Two lines, marking excess rows of bubbles, emerge from each core. (**B**) Domain area histograms (in semilogarithmic representation) with superimposed fits to a single or a superposition of three Gaussians, shifted to a common maximum position: area values for the original maxima are (a) 52, (b) 76, (c) 117, and (d) 245 μm^2. Abscissae were expanded, as indicated by scale bars, by factors of 2 (c) and 5 (d) with respect to those of (a) and (b). Distributions (c) and (d), respectively, correspond to Figs. 1B and 2A, and all histograms are also related to the plots marked (a) through (d) in Fig. 4. Fits yield, for (a), the polydispersity of the initial state, $(\langle A^2 \rangle - \langle A \rangle^2)^{1/2}/\langle A \rangle \approx 0.18$, and, for (d), ratios $R_5/R_6 \approx 0.77$ and $R_6/R_7 \approx 0.88$ for the mean radii of n-fold coordinated bubbles.

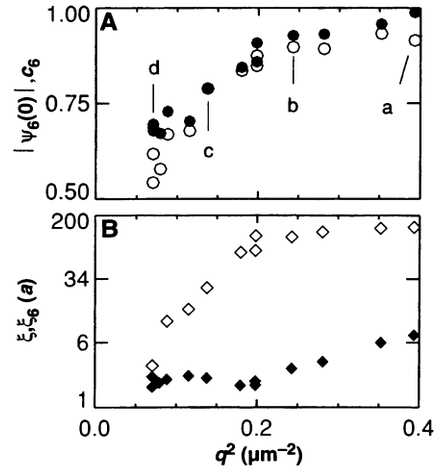

Fig. 4. (**A**) Concentration of sixfold coordinated bubbles, $c_6 \equiv 1 - (N_5 + N_7)/N$ (●), obtained from Voronoi diagrams by omission of sites near edges of the field of view, and absolute value of the orientational order parameter, $|\psi_6| \equiv g_6(0)^{1/2}$ (○). Histograms (a) through (d) in Fig. 3B correspond to patterns as indicated here. (**B**) Translational (ξ; ◆) and orientational (ξ_6; ◇) correlation lengths, in units of the nearest-neighbor distance, a, on a logarithmic scale. The common abscissa is given in terms of the square of the modulation wavevector, $q \equiv |\mathbf{q}_H(T)|$, evaluated from azimuthally averaged Fourier spectra.

correlations even at exceedingly low defect concentrations at high T (see Fig. 1A). Careful examination reveals that the distortions introduced on a scale of many nearest-neighbor distances by even a single, unpaired dislocation (Fig. 1A) lead to a significant reduction of $\xi \approx 10a << \xi_6$ (where a is the distance to the nearest neighbor), in essential agreement with the situation encountered in dilute magnetic bubble arrays at room temperature (*11, 24*). The reduction of the asymptotic value of $|\psi_6|$ to below unity (Fig. 4A) is likewise attributed to the free dislocation and to possible additional static random displacement disorder. Whether a state of true long-range positional order exists in magnetic bubble arrays near T_c remains an open question.

In the final stage, represented by the patterns in Figs. 1C and 2A and characterized by the correlation functions in Fig. 2B, an isotropic, amorphous state of comparable ξ_6 and $\xi \approx \xi_6 \approx 2a$ appears. Close examination of the corresponding Voronoi diagram (Fig. 2A) confirms the incipient unbinding of ± 1 disclinations (*17*), respectively marking five- and sevenfold sites; disclinations of charge exceeding ± 1, commonly observed in other systems (*10, 11, 22*), are not formed here. In a system of colloidal spheres of comparable defect density ($1 - c_6 \approx 0.25$), a significant number of unbound disclinations, exceeding by almost an order of magnitude that found here, ensures realization of a true, isotropic liquid state (*10*). Disclinations in the high-coverage magnetic system here, perhaps as a result of bubble size adjustment, appear to be more tightly bound.

Roughly coincident with the appearance of an amorphous state (Fig. 4), ξ, which tracks the average (lateral) distance between dislocations (*10, 22*), approaches an asymptotic level (*9*). Close inspection of the evolving pattern reveals the activation of an additional mechanism for the elimination of bubbles; this involves the annihilation of interstitials, and hence of dislocation pairs, and thus facilitates local "healing" of the disordered pattern. This process is mediated by the collapse of fivefold coordinated bubbles in a manner closely related to the collapse of five-sided cells in coarsening polygonal networks ("froths") (*9, 25*).

We suggest that, as with the evolution of labyrinthine stripe domain patterns from a lamellar initial state (*9, 26*), the morphology of disordered bubble patterns may be viewed as a configuration of correct modulation period emerging from constrained optimization under the condition of fixed coverage and given number density of bubbles. The possible interplay between the strain relaxation achieved by bubble area adjustment and the dissociation of dislocations into their constituent disclinations, beginning to occur in the most disordered patterns (see Fig. 2A), constitutes an interesting, currently unresolved problem.

"Frustration," arising from quenched size inhomogeneity, and its effect on translational and orientational ordering have been previously examined in binary arrays of spheres, as well as in simulations of close-packed hard disks (*22*), in an effort to understand the evolution of amorphous structures and the connection to melting in two dimensions. Related questions have recently been addressed in the study of three-dimensional spherical colloids; binary mixtures of colloidal spheres of sufficiently different size have in fact been shown to exhibit a glass transition at high densities (*27*). However, in contrast to the quenched disorder pertinent to those situations, we find that polydispersity and thus frustration arise spontaneously in dense magnetic bubble patterns in response to the formation of dislocation cores. This intimate connection between geometry and topology, relating the sites of particles of nonoptimal size to the position of topological defects, yields a simple example of a mechanism generating structural disorder typical of that found in amorphous systems such as glasses (*28*).

REFERENCES AND NOTES

1. T. E. Faber, *Proc. R. Soc. London Ser. A* **248**, 460 (1958).
2. R. E. Rosensweig, M. Zahn, R. J. Shumovich, *J. Magn. Magn. Mater.* **39**, 127 (1983); A. O. Cebers and M. M. Maiorov, *Magnetohydrodynamics* **16**, 21 (1980).
3. J. A. Cape and G. W. Lehman, *J. Appl. Phys.* **42**, 5732 (1971); P. Molho, J. L. Porteseil, Y. Souche, J. Gouzerh, J. C. S. Levy, *ibid.* **61**, 4188 (1987).
4. T. Garel and S. Doniach, *Phys. Rev. B* **26**, 325 (1982).
5. H. Möhwald, *Annu. Rev. Phys. Chem.* **41**, 441 (1990); H. M. McConnell, *ibid.* **42**, 171 (1991).
6. D. Andelman, F. Brochard, J.-F. Joanny, *J. Chem. Phys.* **86**, 3673 (1987).
7. O. Alerhand *et al.*, *Phys. Rev. Lett.* **61**, 1973 (1988); *ibid.* **62**, 166 (1989); D. Vanderbilt, *Surf. Sci. Lett.* **268**, 300 (1992).
8. M. Seul and R. Wolfe, *Phys. Rev. Lett.* **68**, 2460 (1992); *Phys. Rev. A* **46**, 7519 (1992); *ibid.*, p. 7534.
9. M. Seul, in preparation.
10. C. A. Murray and D. H. Van Winkle, *Phys. Rev. Lett.* **58**, 1200 (1987); C. A. Murray, W. O. Sprenger, R. A. Wenk, *Phys. Rev. B* **42**, 688 (1990); C. A. Murray, D. H. Van Winkle, R. A. Wenk, *Phase Transitions* **21**, 93 (1990).
11. R. Seshadri and R. M. Westervelt, *Phys. Rev. Lett.* **66**, 2774 (1991); *Phys. Rev. B* **46**, 5142 (1992); *ibid.*, p. 5150.
12. A. A. Thiele, *J. Appl. Phys.* **41**, 1139 (1970); H. M. McConnell, *J. Phys. Chem.* **94**, 4728 (1990).
13. M. M. Hurley and S. J. Singer, *J. Phys. Chem.* **96**, 1938 (1992); *ibid.*, p. 1951.
14. M. Seul and M. J. Sammon, *Phys. Rev. Lett.* **64**, 1903 (1990); M. Seul, *Physica A* **168**, 198 (1990).
15. S. A. Langer, R. E. Goldstein, D. P. Jackson, *Phys. Rev. A* **46**, 4894 (1992).
16. The pair correlation function, $g(\mathbf{r})$, serves to specify the degree of translational order by measuring the distance dependence of static two-point correlations in the density. The exponential decay of $g(\mathbf{r})$ displayed by fluids defines a characteristic scale for the decay of translational correlations and is denoted by ξ in the text [J. P. Hansen and I. R. McDonald, *Theory of Simple Liquids* (Academic Press, London, 1986)]. Orientational order in two dimensions is measured by a complex hexatic order parameter $\psi_6(\mathbf{r}) \equiv \exp[i6\theta(\mathbf{r})]$. Here θ denotes the angle subtended by nearest-neighbor–connecting lines ("bonds") and the positive x axis, and $\mathbf{r}$ refers to the mid-point of the bond. A quantitative measure of the distance dependence of ϕ_6 is provided by the orientational correlation function $g_6(\mathbf{r}) = \langle \psi_6^*(\mathbf{r})\psi_6(0)\rangle$, with ξ_6 denoting the associated characteristic decay length [D. R. Nelson, in *Phase Transitions and Critical Phenomena*, C. Domb and J. K. Lebowitz, Eds. (Academic Press, London, 1983), vol. 7].
17. Dislocations represent the topological defect of lowest energy of an ordered two-dimensional solid. Each dislocation core is composed of a pair of other point defects, called disclinations, of equal and opposite (topological) charge. A disclination of charge -1 is a particle with five nearest neighbors, and one with charge $+1$ has seven nearest neighbors [N. D. Mermin, *Rev. Mod. Phys.* **51**, 591 (1979)]. Isolated ("unbound") disclinations generate configurations of imperfect local bonding, and the "unbinding" of pairs of such point defects is thought to mediate melting (*10, 11, 16*).
18. This transformation is irreversible: The nucleation of bubbles, required to accommodate lattice compression, is suppressed, and this favors the elongation ("strip-out") of bubbles.
19. M. Seul and V. S. Chen, *Phys. Rev. Lett.* **70**, 1658 (1993).
20. M. Seul, M. J. Sammon, L. R. Monar, *Rev. Sci. Instrum.* **62**, 784 (1991).
21. The Voronoi diagram of a set of points is a planar graph delineating polygonal cells. Each cell is associated with exactly one point, P, in the set and contains the portion of the plane that lies closer to P than to any other member of the set [S. J. Fortune, *Algorithmica* **2**, 153 (1987); D. Weaire and N. Rivier, *Contemp. Phys.* **25**, 59 (1984)].
22. D. R. Nelson, M. Rubinstein, F. Spaepen, *Philos. Mag. A* **46**, 105 (1982); M. Rubinstein and D. R. Nelson, *Phys. Rev. B* **26**, 6254 (1982); G. C. Barker and M. J. Grimson, *J. Phys. C* **1**, 2779 (1989); M. F. Thorpe and Y. Cai, *Phys. Rev. B* **43**, 11019 (1991).
23. Although hexatic orientational correlations are expected (*10, 22*) to decay algebraically, we chose an exponential parametrization to obtain an estimate of correlation length, ξ_6 (Fig. 4).
24. E. M. Chudnovsky, *Phys. Rev. B* **40**, 11355 (1989); *ibid.* **43**, 7831 (1991).
25. In fact, a more fundamental connection has been noted (*29*) between cellular networks and certain bubble patterns such as those in magnetic garnet and in Langmuir films (*5, 14, 30*): all belong to a family of patterns described by a common topology, here that of a planar triangulation, and a scalar field defined on that topology, here the set of domain areas.
26. M. Seul, L. R. Monar, L. O'Gorman, R. Wolfe, *Science* **254**, 1616 (1991); M. Seul, L. R. Monar, L. O'Gorman, *Philos. Mag. B* **66**, 471 (1992).
27. P. N. Pusey, *J. Phys. Paris* **48**, 709 (1987); P. Bartlett, R. H. Ottewill, P. N. Pusey, *J. Chem. Phys.* **93**, 1299 (1990); R. McRae and D. J. Haymet, *ibid.* **88**, 1114 (1988).
28. D. R. Nelson, in *Phase Transitions and Critical Phenomena*, C. Domb and J. K. Lebowitz, Eds. (Academic Press, London, 1983), vol. 12.
29. M. Magnasco, *Philos. Mag. B* **65**, 895 (1992).
30. B. Berge, A. Simon, A. Libchaber, *Phys. Rev. A* **41**, 6893 (1990); K. Stine *et al.*, *ibid.*, p. 6884.

31. Various aspects of this work have benefitted from conversations with D. Huse and R. Wolfe.

11 June 1993; accepted 23 August 1993